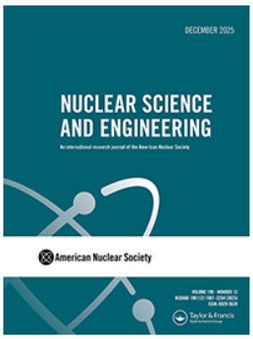

Nuclear Science and Engineering

ISSN: 0029-5639 (Print) 1943-748X (Online) Journal homepage: www.tandfonline.com/journals/unse20

A Flexible, Moment-Preserving, and Monotone Discretization of the Multidimensional Angular Fokker–Planck Operator

Charles Bienvenue, Ahmed Naceur, Jean-François Carrier & Alain Hébert

To cite this article: Charles Bienvenue, Ahmed Naceur, Jean-François Carrier & Alain Hébert (08 Apr 2025): A Flexible, Moment-Preserving, and Monotone Discretization of the Multidimensional Angular Fokker–Planck Operator, Nuclear Science and Engineering, DOI: 10.1080/00295639.2025.2462891

To link to this article: https://doi.org/10.1080/00295639.2025.2462891

NUCLEAR SCIENCE AND ENGINEERING

DOI: https://doi.org/10.1080/00295639.2025.2462891

A Flexible, Moment-Preserving, and Monotone Discretization of the Multidimensional Angular Fokker–Planck Operator

Charles Bienvenue,[a]* Ahmed Naceur,[a] Jean-François Carrier,[b] and Alain Hébert[a]

[a]*Polytechnique Montréal, Institut de génie nucleaire, Montréal H3C 3A7, Canada*
[b]*Université de Montréal, Département de physique, Montréal H3T 1J4, Canada*

Received August 12, 2024
Accepted for Publication January 18, 2025

Abstract — *A monotone finite-difference scheme is proposed for the multidimensional angular Fokker–Planck operator in discrete ordinates calculations. It is compatible with nonorthogonal quadrature sets on the unit sphere and preserves the null space, the zeroth, and the first three angular moments of the analytical angular Fokker–Planck operator. Numerical results demonstrate that this discretization, combined with the suitable Galerkin quadrature method, eliminates spurious oscillations in the flux solution related to highly anisotropic scattering.*

Keywords — *Transport equation, discrete ordinates, Fokker–Planck operator, finite-difference schemes.*

Note — *Some figures may be in color only in the electronic version.*

I. INTRODUCTION

Angular discretization of the transport equation by the discrete ordinates (S_N) method leads to numerical issues. In the presence of highly forward-peaked scattering, the S_N method can produce highly inaccurate solutions, but with Gauss-Legendre quadrature in one-dimensional (1D) geometry.[1] Pautz and Adams showed that the source iteration process can even diverge, notably in scattering-dominated medium.[2] Such divergence is due to inappropriate angular discretization approximations, which can introduce a nonphysical multiplication factor in the medium, leading to an absence of a steady-state solution.

The Galerkin quadrature methodology has been developed to tackle these issues and to make the S_N method robust.[1,3] However, the Galerkin method does not provide a monotone representation of the angular flux scattering.[4,5] Undesirable numerical artifacts still can appear in the solution, such as rather important oscillations in the presence of anisotropic scattering, distinct from the well-known ray effects in multidimensional transport.[6]

The purpose of this paper is to propose a methodology to mitigate these monotonicity issues related to highly anisotropic scattering using the angular Fokker–Planck (AFP) operator. Following the work of Landesman and Morel, the forward-peaked elastic scattering handling can be transferred from the Boltzmann operator to the AFP operator, for which monotone and moment-preserving finite-difference schemes exist.[7] For the 1D AFP operator, the finite-difference scheme from Morel,[8] applicable to any choice of quadrature, is used. For the multidimensional AFP operator, a finite-difference scheme is developed based on the Voronoi tessellation of the unit sphere.[9] This scheme is a generalization of the previous work of Morel et al.,[10] with product quadrature sets to nonorthogonal quadrature sets on the unit sphere.

This paper is organized as follows. In Sec. II, we describe the Boltzmann Fokker–Planck (BFP) equation, which

*E-mail: charles.bienvenue@polymtl.ca
Supplemental data for this article can be accessed online at https://doi.org/10.1080/00295639.2025.2462891

contains the ingredients of the angular discretization proposed in this work. In Sec. III, the discrete ordinates and Galerkin quadrature method formalism is introduced. In Sec. IV, finite-difference schemes for the Fokker–Planck (FP) operator are developed to be compatible with nonorthogonal quadrature sets. Finally, in Sec. V, the impacts of the proposed methodology for angular discretization on energy deposition benchmarks are presented and discussed.

II. BFP EQUATION

The presented angular discretization is based on the BFP equation, which consists of the linear Boltzmann transport equation to which FP terms are added. Przybylski and Ligou introduced it to deal accurately with both small and large energy loss interactions by having specific treatment for each of them.[11] The main idea is that interactions leading to small energy losses and angular deflection, called soft interactions, are handled by the FP operator, while interactions leading to large energy transfer, called catastrophic interactions, are handled by the Boltzmann operator. The FP operator is an asymptotic limit of the Boltzmann operator for small energy loss and direction change.[12]

Let $\mathbb{S}^2 = \{\Omega = (\mu, \eta, \xi) \in \mathbb{R}^3 : ||\Omega|| = 1\}$ be the unit sphere, Ω the particle direction, and $\mu, \eta, \xi \in [-1, 1]$ the direction cosines along *x-*, *y-*, and *z*-axis, respectively. Let E be the particle energy, and $\mathbf{r} = (x, y, z) \in \mathbb{R}^3$ be the particle position. The steady-state BFP equation is given by

$$\begin{aligned}\Omega \cdot \nabla\Psi(\boldsymbol{r}, \Omega, E) + \Sigma_t(\boldsymbol{r}, E)\Psi(\boldsymbol{r}, \Omega, E) \\ = Q^{\mathrm{FP}}(\boldsymbol{r}, \Omega, E) + Q^{\mathrm{B}}(\boldsymbol{r}, \Omega, E) + Q^{ext}(\boldsymbol{r}, \Omega, E) \ , \end{aligned} \tag{1}$$

where $Q^{ext}(\mathbf{r}, \Omega, E)$ consists of fixed external sources of particles. The FP operator, with respectively the continuous slowing-down (CSD) and AFP terms, is given by[13]

$$Q^{\mathrm{FP}}(\boldsymbol{r}, \Omega, E) = Q^{\mathrm{CSD}}(\boldsymbol{r}, \Omega, E) + Q^{\mathrm{AFP}}(\boldsymbol{r}, \Omega, E) \ , \tag{2}$$

where

$$\begin{aligned} &Q^{\mathrm{CSD}}(\boldsymbol{r}, \Omega, E) = \frac{\partial}{\partial E}\left[S(\boldsymbol{r}, E)\Psi(\boldsymbol{r}, \Omega, E)\right] \\ &\text{and} \quad Q^{\mathrm{AFP}}(\boldsymbol{r}, \Omega, E) = T(\boldsymbol{r}, E)\nabla_\Omega^2\Psi(\boldsymbol{r}, \Omega, E) \ . \end{aligned} \tag{3}$$

The Boltzmann operator, in which scattering cross sections are expanded in Legendre polynomials and angular flux are expanded in N_p spherical harmonics, is[14]

$$\begin{aligned} Q^{\mathrm{B}}(\boldsymbol{r}, \Omega, E) = \int_0^\infty dE' \sum_{p=1}^{N_p} \frac{2\ell_p + 1}{4\pi} \Sigma_{s,\ell_p}(\boldsymbol{r}, E' \to E) \\ R_{\ell_p}^{m_p}(\Omega)\Phi_p(\boldsymbol{r}, E') \ , \end{aligned} \tag{4}$$

with the angular flux moments

$$\Phi_p(\boldsymbol{r}, E') = \int_{\mathbb{S}^2} d^2\Omega' R_{\ell_p}^{m_p}(\Omega')\Psi(\boldsymbol{r}, \Omega', E') \ , \tag{5}$$

where

$R_\ell^m(\Omega)$ = real spherical harmonics, as defined in Hébert[14] using Ferrer definitions of the associated Legendre polynomials

$\Psi(\mathbf{r}, \Omega, E)$ = angular flux

$\Sigma_t(\mathbf{r}, E)$ = macroscopic total cross section

$\Sigma_{s,\ell}(\mathbf{r}, E' \to E)$ = ℓ-order Legendre moment of the macroscopic scattering cross section from energies E' to E

$S(\mathbf{r}, E)$ = soft stopping power

$T(\mathbf{r}, E)$ = soft momentum transfer.

For a more formal definition of the cross sections, stopping powers, and momentum transfer in the BFP, as well as the definition of the soft and catastrophic interactions, see Refs. [15,16]. The indexes ℓ_p and m_p are functions of their index p, whose values are given following a Gramm-Schmidt process to select a subset of spherical harmonics, as described in Sec. III.

The multigroup discretization of Eq. (1), which divides the energy domain into G energy groups, and the discretization schemes for both streaming (spatial derivative) and CSD terms (energy derivative), are described in previous works[4,11,15,17–19] and are not the focus of this paper.

This paper aims to propose a flexible angular discretization framework that capitalizes on the capacities of the BFP equation, based on its AFP and Boltzmann operators. Note that while the CSD term is employed in this work for electron transport, the presented method does not rely on it. The following schemes could equally be applied to the Boltzmann equation by including the AFP operator in it, and could equally be applied to neutral particle transport. Particularly, it could be of interest for very fast neutron transport using discrete ordinate solvers.[20]

The elastic scattering cross sections can be decomposed into soft and catastrophic components.[7] Let's assume

a material identified by index i. Let L be the order of the cross section Legendre expansion and $\Sigma_{s,\ell,i}^{g\to g}$ be the ℓ-order Legendre moment of the elastic scattering cross section in group g in material i. Let $L_{max} \leq L$ be the last nonzero Legendre moments of the scattering in group g in material i. The Legendre moments of the soft are assumed to be given by

$$\Sigma_{s,\ell,i}^{g\to g,soft} = \Sigma_{s,0,i}^{g\to g,soft} - T_{g,i}\ell(\ell+1) \tag{6}$$

for $\ell \in \{1, ..., L_{max}\}$. This expression is obtained by establishing equality between the eigenvalues of the Boltzmann and the AFP operator applied to the Legendre polynomials.[13]

This method sets a relation that depends on two undefined parameters $\Sigma_{s,0,i}^{g\to g,soft}$ and $T_{g,i}$, which are defined to ensure the preservation of the Boltzmann operator moments by the FP operator. Landesman and Morel proposed to equate $\Sigma_{s,L_{max}-1,i}^{g\to g,soft} = \Sigma_{s,L_{max}-1,i}^{g\to g}$ and $\Sigma_{s,L_{max},i}^{g\to g,soft} = \Sigma_{s,L_{max},i}^{g\to g}$ to define these parameters, which results in

$$T_{g,i} = \frac{\Sigma_{s,L_{max}-1,i}^{g\to g} - \Sigma_{s,L_{max},i}^{g\to g}}{2L_{max}} \tag{7}$$

and

$$\Sigma_{s,0,i}^{g\to g,soft} = \Sigma_{s,L_{max},i}^{g\to g} + T_{g,i}L_{max}(L_{max}+1)\ . \tag{8}$$

The soft component of the elastic cross sections should then be withdrawn from cross sections since the AFP operator, jointly with the momentum transfer given by Eq. (7), is used to treat that soft scattering. The resulting catastrophic cross sections are given by

$$\Sigma_{s,\ell,i}^{g\to g,catas} = \Sigma_{s,\ell,i}^{g\to g} - \Sigma_{s,\ell,i}^{g\to g,soft}\ . \tag{9}$$

The Legendre moments of the cross sections are obtained by substituting Eqs. (8) and (6) into Eq. (9). Thus, the total elastic cross sections are redefined as

$$\Sigma_{t,g,i}^{catas} = \Sigma_{t,g,i} - \Sigma_{s,L_{max},i}^{g\to g} - T_{g,i}L_{max}(L_{max}+1)\ , \tag{10}$$

and the ℓ-order Legendre moment of the scattering cross sections are redefined as

$$\Sigma_{s,\ell,i}^{g\to g,catas} = \Sigma_{s,\ell,i}^{g\to g} - \Sigma_{s,L_{max},i}^{g\to g} - T_{g,i}[L_{max}(L_{max}+1) - \ell(\ell+1)]\ . \tag{11}$$

This method, as presented, includes the extended transport correction.[21,22] The goal of this operation is to transfer the handling of forward-peaked scattering from the Boltzmann operator, which encounters monotonicity issues with such scattering,[4] to the FP operator, which can be tackled by finite-difference discretization schemes.[8,10]

III. DISCRETE ORDINATES METHOD AND GALERKIN QUADRATURE

The discrete ordinates method, also known as the S_N method, consists of the discretization of the angular domain and the unit sphere $\mathbb{S}^2$ in the N_d discrete directions Ω_n for $n = \{1, ..., N_d\}$. Numerical quadrature is used to deal with integrals over $\mathbb{S}^2$ using weights w_n associated with each direction Ω_n. The S_N equations are obtained by requiring the one-speed transport equation in group g to hold when evaluated at each Ω_n, such as

$$\Omega_n \cdot \nabla\Psi_{g,n}(\boldsymbol{r}) + \Sigma_{t,g}\Psi_{g,n}(\boldsymbol{r}) = Q_{g,n}^{\mathrm{CSD}}(\boldsymbol{r}) + Q_{g,n}^{\mathrm{AFP}}(\boldsymbol{r}) + Q_{g,n}^{\mathrm{B}}(\boldsymbol{r}) + Q_{g,n}^{ext}(\boldsymbol{r})\ , \tag{12}$$

where the Boltzmann operator is given by

$$Q_{g,n}^{\mathrm{B}}(\boldsymbol{r}) = \sum_{g'=1}^{G}\sum_{p=1}^{N_p}\frac{2\ell_p+1}{4\pi}\Sigma_{s,\ell_p}^{g'\to g}(\boldsymbol{r})R_{\ell_p}^{m_p}(\Omega_n)\Phi_{g',p}(\boldsymbol{r})\ , \tag{13}$$

with g' and g being the energy group of the incoming and outgoing particle, and where

$$\Phi_{g',p}(\boldsymbol{r}) = \sum_{n=1}^{N_d}\omega_n R_{\ell_p}^{m_p}(\Omega_n)\Psi_{g',n}(\boldsymbol{r})\ . \tag{14}$$

The AFP operator discretization is given in Sec. IV. The CSD operator discretization is not discussed here since it is independent of the proposed angular discretization; see Refs. [11,17,18] for a detailed treatment of that operator. The S_N method leads to a set of N_d equations that can be solved using iterative techniques. At each iteration, along each direction, the flux solution is computed across the spatial domain in a process, often referred to as sweeping,[14] using the most up-to-date particle sources.

Then the sources are actualized using the last estimation of the flux solution. To achieve this, the N_d discrete angular fluxes in $\Psi_g = \left(\Psi_{g,1}, \Psi_{g,2}, ..., \Psi_{g,N_d}\right)$ have to be converted in N_p spherical harmonics flux moments in $\Phi_g = \left(\Phi_{g,1}, \Phi_{g,2}, ..., \Phi_{g,N_p}\right)$. The resulting spherical harmonics flux moments are multiplied by their corresponding Legendre moments of the scattering cross section to obtain

the Legendre moments of the Boltzmann sources, which are then converted back into discrete angular sources for the following iteration. These conversion operations can be expressed in matrix form using both the discrete-to-moment **D** and the moment-to-discrete **M** matrices such as

$$\Phi_g = \mathbf{D}\Psi_g \quad \text{and} \quad \Psi_g = \mathbf{M}\Phi_g \ . \tag{15}$$

The standard discrete ordinates conversion matrix components are given by

$$D_{p,n} = w_n R_{\ell_p}^{m_p}(\Omega_n)$$

and

$$M_{n,p} = \frac{2\ell_p + 1}{4\pi} R_{\ell_p}^{m_p}(\Omega_n) \tag{16}$$

for $n = 1, N_d$ and $p = 1, N_p$. In 1D Cartesian geometry, these conversion matrix components can be reduced to

$$D_{p,n} = w_n P_{\ell_p}(\mu_n)$$

and

$$M_{n,p} = \frac{2\ell_p + 1}{2} P_{\ell_p}(\mu_n) \ , \tag{17}$$

where $P_{\ell_p}(\mu_n)$ are Legendre polynomials and $\ell_p = p - 1$.

The quadrature on the unit sphere reduces to a quadrature over the direction cosine μ domain, which spans from −1 to 1. With these matrices, the vector containing the N_d Boltzmann sources, $\boldsymbol{Q}_g^B = \left(Q_{g,1}^{\mathrm{B}}, Q_{g,2}^{\mathrm{B}}, ..., Q_{g,N_d}^{\mathrm{B}}\right)$, is given by

$$\boldsymbol{Q}_g^{\mathrm{B}} = \sum_{g'=1}^{G} \mathbf{M}\, \Sigma^{g' \to g} \mathbf{D} \Psi_{g'} \ , \tag{18}$$

where $\boldsymbol{\Sigma}^{g' \to g}$ is a $N_p \times N_p$ diagonal matrix with each component associated with ℓ_p-order Legendre moments of the scattering cross section ($\Sigma_{p,p}^{g' \to g} = \Sigma_{s,\ell_p}^{g' \to g}$).

The definition of indexes ℓ_p and m_p depending on index p can seem messy, but it is a compact and versatile notation that enables any choice of a subset of spherical harmonics. For instance, based on Reed's S_2 suitable interpolation basis for level-symmetric quadrature in two-dimensional (2D) Cartesian geometry,[23] composed of R_0^0, R_1^0, R_1^1, and R_2^1, the corresponding indexes are given by $\ell = (0, 1, 1, 2)$ and $\mathbf{m} = (0, 0, 1, 1)$, and the diagonal of the $\Sigma^{g' \to g}$ matrix is given by $(\Sigma_{s,0}^{g' \to g}, \Sigma_{s,1}^{g' \to g}, \Sigma_{s,1}^{g' \to g}, \Sigma_{s,2}^{g' \to g})$.

It is well known that there is an equivalence in 1D Cartesian or spherical geometry between the discrete ordinates solution, using the N-order Gauss-Legendre quadrature with Legendre expansion of degree $N - 1$, and the $(N - 1)$-order spherical harmonics (or P_N) solution using Mark boundary conditions.[13,14] In fact, with such quadrature and Legendre expansion, both conversion matrices **M** and **D** are square and inverse of each other, which is very desirable since it ensures accurate integration regardless of the strength of the anisotropy.[4] This ensures an exact integration of a Dirac scattering and that the commonly used transport correction leaves the solution of the transport equation invariant, which is not the case with any other quadrature choice.[1]

This is a major shortcoming in multidimensional geometries since there is no known quadrature on the unit sphere or choice of polynomial basis that results naturally to conversion matrices that are inverse of each other. While the classical S_N method can lead to inaccurate and nonphysical solutions, it also can prevent convergence by allowing a scattering ratio to exceed one, which mostly happens in scattering-dominated mediums.[2] Such a scattering ratio is associated with each scattering moment, and a single discrepancy is sufficient to disrupt the iterative process. These problems become apparent when dealing with charged particles, for which scattering is dominant and scattering is highly forward peaked.

The Galerkin quadrature method, developed by Morel, solves the most important issues of the classical S_N method.[1,3] It ensures the exact integration of a Dirac scattering, and as a corollary, that the transport correction leaves the solution of the transport equation invariant.[4] It guarantees that the scattering ratios remain below one for all moments, thereby ensuring proper convergence of the source iteration process.[2] The Galerkin method, however, does not offer a solution to artifacts related to scattering positivity.[1] A Galerkin quadrature is obtained by inverting either the discrete-to-moment or the moment-to-discrete matrix, evaluated using Eqs. (16) or (17), i.e.,

$$\mathbf{D} = \mathbf{M}^{-1} \ . \tag{19}$$

This requires that **D** and **M** are square and invertible matrices. If we can compute **M** with these two properties, it can be inverted to find **D**, or vice versa, to obtain a Galerkin quadrature.[1,3,24] For these matrices to be square, the number of directions N_d (nodes of the quadrature) has to be strictly equal to the number of basis functions used in the angular flux expansion. To be invertible, linearly independent matrix columns are required, which is not the case for every choice of basis functions. While it is not part of the present work, the

reader should also be aware that Shands et al.[3] have developed a new Galerkin quadrature method that eliminates the need for matrix inversion.

For 1D Cartesian geometries, Legendre polynomials can be used as basis functions. For a quadrature with N_d nodes, the Legendre polynomials up to order $N_d - 1$ should be chosen as the basis function of the angular flux expansion. The discrete-to-moment matrix $\mathbf{D}$ can then be computed using Eq. (17), and it can be inverted to obtain the moment-to-discrete matrix $\mathbf{M}$, or vice versa, without any additional difficulties. This is because the previously stated choice of Legendre polynomials yields square and invertible matrices. The Gauss-Legendre quadrature is the sole quadrature choice that naturally produces a Galerkin quadrature with classical S_N.[13] The Galerkin quadrature method allows for the use of the Gauss–Lobatto quadrature, which is very useful when dealing with normally incident particle sources due to its two nodes aligned with the Cartesian reference system axis ($\mu = -1$ and $\mu = 1$).[4]

For multidimensional geometries, the real spherical harmonics are used as basis functions. For a quadrature set with N_d nodes, a subset of spherical harmonics has to be chosen knowing that not every subset leads to an invertible discrete-to-moment matrix (or vice versa). While rules for a suitable subset of spherical harmonics exist for some quadrature sets,[1,3,25] a Gram–Schmidt procedure has been proposed by Drumm et al. to choose a subset of spherical harmonics such that the columns of $\mathbf{D}$ (or $\mathbf{M}$) are linearly independent, regardless of the choice of quadrature.[26,27] This procedure, which is described in Algorithm 1, was employed in this work. It should be noted that quadrature on the unit sphere and real spherical harmonics basis functions can also be used in 1D geometry.

Algorithm 1 Gram–Schmidt procedure for selecting a suitable subset of spherical harmonics to ensure invertibility of the discrete-to-moment $\mathbf{D}$ or the moment-to-discrete $\mathbf{M}$ matrices, considering machine precision ε and geometry dimension N_{dim}.

$(\boldsymbol{\ell}[1], \mathbf{m}[1]) \leftarrow (0, 0)$
for $\ell \in \{1, ..., N_d\}$ **do**
  $\mathbf{D}[1, n] \leftarrow \omega_n R_0^0(\boldsymbol{\Omega}_n)$ or $\mathbf{M}[n, 1] \leftarrow \frac{1}{4\pi} R_0^0(\boldsymbol{\Omega}_n)$
  $\mathbf{v}_1[n] \leftarrow R_0^0(\boldsymbol{\Omega}_n)$
  $\mathbf{u}_1[n] \leftarrow \mathbf{v}_1[n] / \|\mathbf{v}_1\|$
end for
$i \leftarrow 1$
for $\ell \in \{1, ..., L_{\texttt{max}}\}$ **do**
  if $N_{\text{dim}} = 2$ **then** $m_{\min} = 0$ **else if** $N_{\text{dim}} = 3$ **then** $m_{\min} = -\ell$ **end if**
  for $m \in \{m_{\min}, ..., \ell\}$ **do**
    for $\ell \in \{1, ..., N_d\}$ **do**
      $\mathbf{v}_{i+1}[n] \leftarrow R_\ell^m(\boldsymbol{\Omega}_n)$
    end for
    $\mathbf{v}_{i+1} \leftarrow \mathbf{v}_{i+1} - \sum_{n=1}^{i} \langle \mathbf{u}_n, \mathbf{v}_{i+1} \rangle \mathbf{u}_n$
    if $\|\mathbf{v}_{i+1}\| > \epsilon$ **then**
      $(\boldsymbol{\ell}[i+1], \mathbf{m}[i+1]) \leftarrow (\ell, m)$
      for $\ell \in \{1, ..., N_d\}$ **do**
        $\mathbf{D}[i+1, n] = \omega_n R_\ell^m(\boldsymbol{\Omega}_n)$ or $\mathbf{M}[n, i+1] \leftarrow \frac{2\ell+1}{4\pi} R_\ell^m(\boldsymbol{\Omega}_n)$
        $\mathbf{u}_{i+1}[n] = \mathbf{v}_{i+1}[n] / \|\mathbf{v}_{i+1}\|$
      end for
      $i \leftarrow i + 1$
    end if
    if $i = N_d$ **then return** ($\mathbf{D}$ or $\mathbf{M}$, $\boldsymbol{\ell}$ and $\mathbf{m}$) **end if**
  end for
end for

The efficiency of a quadrature set defined over the unit sphere with N_d nodes that integrate a subspace of spherical harmonics of maximum degree N is given by[28]

$$\eta = \frac{(N+1)^2}{3N_d} \ . \tag{20}$$

A quadrature set is considered optimal if $\eta \approx 1$, and suboptimal if $\eta < 1$. An optimal quadrature set is desirable in S_N transport calculations because the multiplication of nodes increases the number of required sweeps over the spatial domain per iteration to achieve a specific accuracy. The most straightforward quadrature over the sphere is a product quadrature, which consists of the product of two quadrature sets over a line segment along the μ and ϕ coordinates. This quadrature, with $N_d = 2N^2$ nodes, divides the angular domain into orthogonal meshes. However, accurate calculations with such a quadrature set are exceedingly expensive because the quadrature efficiency is constrained between $\eta = 1/6$ $(N \to \infty)$ and $\eta = 3/8$ $(N = 2)$, as shown in Fig. 1.

The node distribution over the sphere is far from uniform with dense pileups of nodes near $\mu = \pm 1$ while it also lacks fourfold ($\mathbf{C}_4$) rotational symmetry around the three axes, as can be seen in Fig. 2. To deal with these issues, the so-called level-symmetric quadrature sets were developed. An example is Carlson's ES_N quadrature,[29] which presents a more uniform node distribution and $\mathbf{C}_4$ rotational symmetry around the axis. It has $N_d = N(N+2)$, and the resulting efficiency of this kind of quadrature still is constrained between $\eta = 1/3$ $(N \to \infty)$ and $\eta = 3/8$ $(N = 2)$.

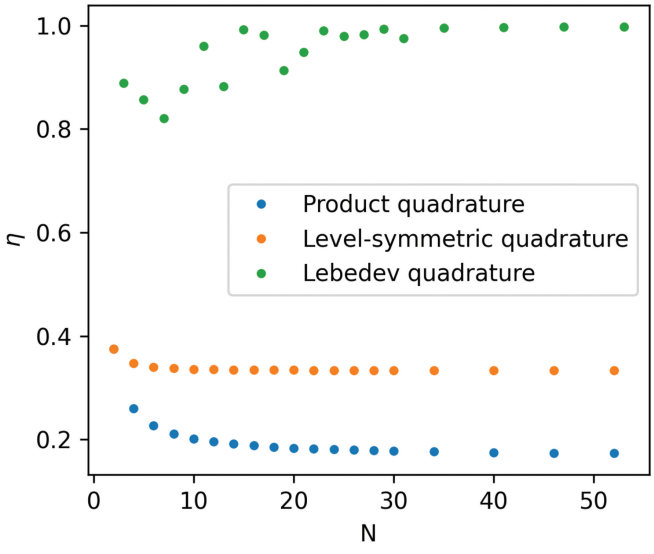

Fig. 1. Quadrature efficiency of the product quadrature (Gauss–Legendre quadrature along μ and Chebychev quadrature along ϕ), the level-symmetric quadrature (Carlson ES_N quadrature), and the Lebedev quadrature.

Optimal, or sightly optimal, quadrature sets do exist, such as the ones of Lebedev[30,31] and Lebedev and Laikov.[32] These quadratures possess octahedral rotation symmetry with inversion, and have as the Gauss–Lobatto in 1D, nodes along the Cartesian reference system axis.[30] While these nodes along the axis are useful for treating normally incident beams, they lead to an asymmetric subset of spherical harmonics for the Galerkin quadrature methods, which is not ideal (see p. 141 of Ref. [25]).

IV. FINITE-DIFFERENCE SCHEMES FOR THE AFP TERM

Extracting the momentum transfer term from the cross sections to treat the elastic forward-peaked scattering with the AFP operator rather than the Boltzmann operator allows for the use of finite-difference schemes to enforce the positivity and monotonicity of the forward-peaked scattering. The N_d FP angular sources are given by

$$\boldsymbol{Q}_g^{\mathrm{AFP}} = T_g \mathcal{M} \boldsymbol{\psi}_g \ , \tag{21}$$

where T_g is the momentum transfer defined in Sec. II and the square $N_d \times N_d$ mapping matrix $\mathcal{M}$ defines the FP scattering between the N_d angular flux. It is worth noting that unlike T_g, $\mathcal{M}$ is independent of energy and position, and therefore needs to be computed only once before the iterative process. Leaving the forward-peaked part of the elastic scattering in the cross sections is equivalent to extracting the momentum transfer from the cross sections and computing the AFP source using the following mapping matrix[5,7]:

$$\mathcal{M} = \mathbf{M} \boldsymbol{\Sigma}^{\mathrm{AFP}} \mathbf{D},$$

with

$$\Sigma_{n,p}^{\mathrm{AFP}} = \begin{cases} -\ell_p(\ell_p+1) & \text{if} \quad n = p \\ 0 & \text{otherwise} \ , \end{cases} \tag{22}$$

where $\mathbf{M} = \mathbf{D}^{-1}$ based on the Galerkin quadrature method. This will be referred to as the Galerkin scheme. It preserves the moments of the AFP operator with the selected subset of spherical harmonics, but it does not yield a monotone mapping matrix $\mathcal{M}$ as does the following finite-difference scheme.

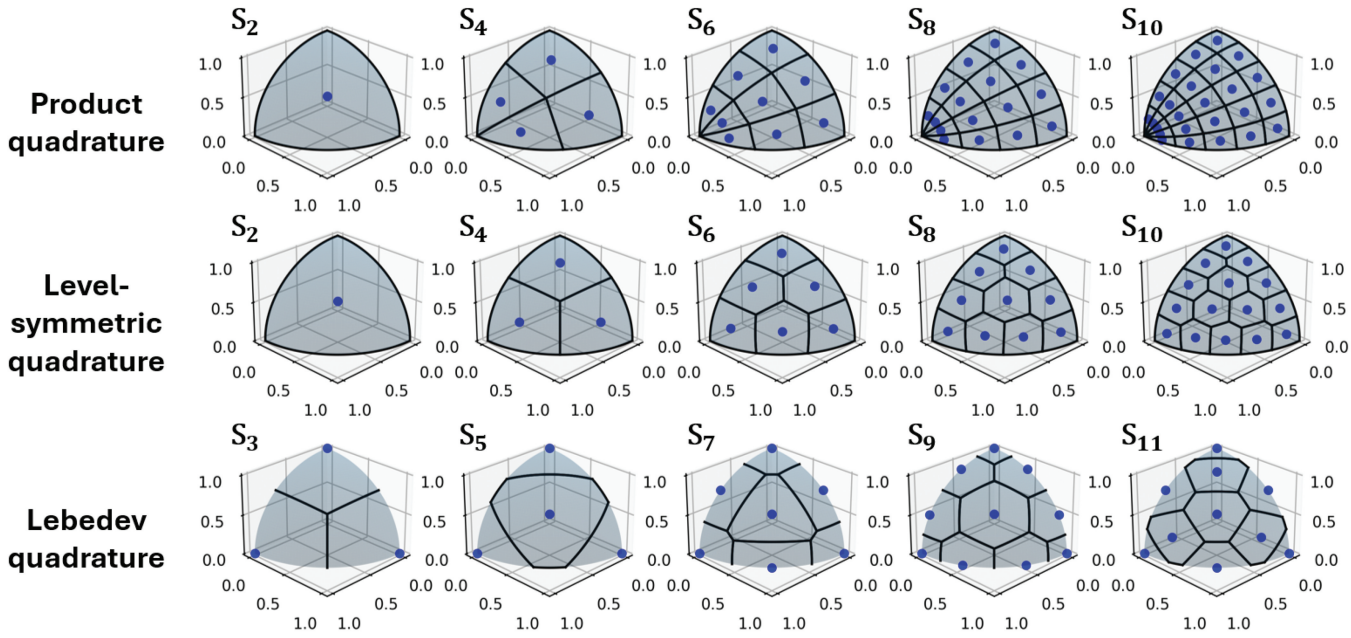

Fig. 2. Voronoi tessellation of the unit sphere positive octant based on the nodes (in blue) of product quadrature (Gauss -Legendre quadrature along μ and Chebychev quadrature along ϕ), level-symmetric quadrature (Carlson ES_N quadrature), and Lebedev quadrature.

IV.A. Finite-Difference Scheme for the 1D AFP Operator

Morel has developed a finite-difference scheme for the 1D AFP operator that preserves both the zeroth and first angular moments of the analytical AFP operator.[7,8] The resulting mapping matrix is a tridiagonal matrix in which components are given by

$$\mathcal{M}_{n,m} = \begin{cases} -C_n & \text{if } n = m \\ C_n^- & \text{if } n = m+1 \\ C_n^+ & \text{if } n = m-1 \\ 0 & \text{otherwise} \end{cases} , \tag{23}$$

where the terms are defined by

$$\begin{aligned} C_n^- &= \frac{C_{n-1/2}}{w_n(\mu_n - \mu_{n-1})} , \\ C_n^+ &= \frac{C_{n+1/2}}{w_n(\mu_{n+1} - \mu_n)} , \end{aligned} \tag{24}$$

and

$$C_n = C_n^- + C_n^+ ,$$

with the recursion formula

$$C_{n+1/2} = C_{n-1/2} - 2\mu_n w_n \quad \text{and} \quad C_{\frac{1}{2}} = 0 . \tag{25}$$

The matrix $\mathcal{M}$ is negative semidefinite (real eigenvalues less or equal to zero) and monotone (negative diagonal and positive off-diagonal elements). This discretization scheme can be described as positive since it will yield positive FP angular sources given positive angular flux.[4,8] This scheme is compatible with any choice of quadrature set.

IV.B. Finite-Difference Scheme for the Multidimensional AFP Operator

Morel et al. have extended the 1D finite-difference FP scheme to multidimensional geometries.[4,10] The proposed scheme, however, is constrained to product quadrature, generating angular mesh boundaries that are aligned with director cosine μ and azimuthal angle ϕ. When the product quadrature is constructed with the Chebychev azimuthal quadrature, it enforces the preservation of the zeroth and the three first angular moments of the AFP operator.

The resulting mapping matrix $\mathcal{M}$ components, over two-dimensional (2D) and three-dimensional (3D) quadrature, are given in the Appendix. It is negative semidefinite, it is monotone, and it yields positive sources. However, as underlined in the previous section, product quadrature sets are far from optimal quadrature ones, as their nodes are unevenly distributed on the sphere and they lack $\mathbf{C}_4$ rotational symmetry around the axes. Using

such quadrature in transport calculations is extremely inefficient due to the enormous amount of nodes Ω_n required to achieve a specific level of angular accuracy, which involves sweeping over the spatial domain for each of these directions. To tackle these shortcomings, we have extended the approach to nonorthogonal quadrature on the unit sphere.

The AFP operator $Q_g^{\mathrm{AFP}}(\Omega)$ is given by[9,33]

$$Q_g^{\mathrm{AFP}}(\Omega) = T_g \nabla_\Omega^2 \Psi_g(\Omega) = T_g \nabla_t \cdot \nabla_t \Psi_g(\Omega) \ , \tag{26}$$

where ∇_Ω^2 is the Laplace operator and ∇_t is the tangential gradient on the unit sphere $\mathbb{S}^2$ given by

$$\nabla_t \Psi_g(\Omega) = \nabla \Psi_g(\Omega) - \left[\nabla \Psi_g(\Omega) \cdot \boldsymbol{n}(\Omega)\right] \boldsymbol{n}(\Omega) \ , \tag{27}$$

where ∇ is the usual gradient in $\mathbb{R}^3$ and $\mathbf{n}(\Omega)$ is the unit normal vector on $\mathbb{S}^2$ at Ω. The integration of the AFP operator over the unit sphere [leftmost expression in Eq. (28)] can be described either as the sum of the integral over N_d nonoverlapping regions Ω_n covering the totality of $\mathbb{S}^2$ [middle expression in Eq. (28)] or by numerical quadrature on $\mathbb{S}^2$ [rightmost expression in Eq. (28)], such as

$$\begin{aligned} \int_{\mathbb{S}^2} d^2\Omega Q_g^{\mathrm{AFP}}(\Omega) &= \sum_{n=1}^{N_d} \int_{\boldsymbol{\Omega}_n} d^2\Omega Q_g^{\mathrm{AFP}}(\Omega) \\ &= \sum_{n=1}^{N_d} \omega_n Q_{g,n}^{\mathrm{AFP}} \ , \end{aligned} \tag{28}$$

where ω_n are the quadrature weights and $Q_{g,n}^{\mathrm{AFP}}$ is the discretized AFP operator.

An example of such N_d nonoverlapping regions over $\mathbb{S}^2$ is given in Fig. 3. This discretized operator can be deduced by association from the previous equation and the integral over region Ω_n can be simplified using divergence theorem over the spherical domain,[33,34]

$$\begin{aligned} Q_{g,n}^{\mathrm{AFP}} &= \frac{1}{\omega_n} \int_{\boldsymbol{\Omega}_n} d^2\Omega Q_g^{\mathrm{AFP}}(\Omega) \\ &= \frac{T_g}{\omega_n} \oint_{\boldsymbol{d\Omega}_n} d\ell \nabla_t \Psi_g(\Omega) \cdot \boldsymbol{n}_\ell \ , \end{aligned} \tag{29}$$

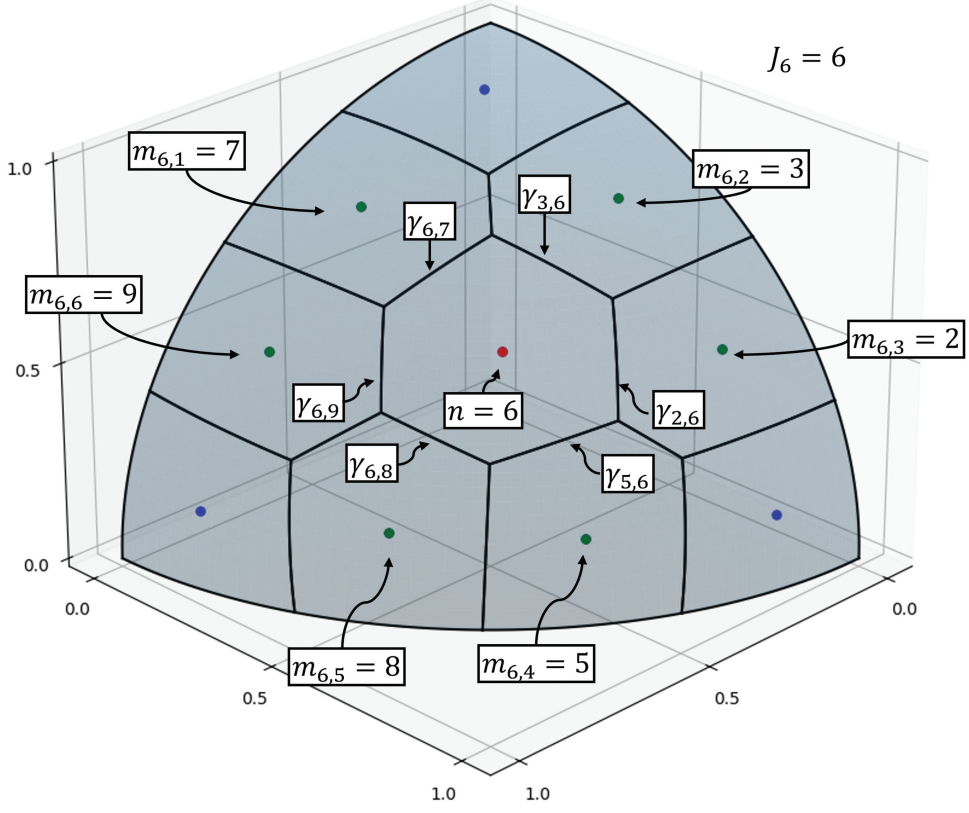

Fig. 3. Voronoi tessellation of the S_8 Carlson's level-symmetric quadrature nodes on the positive octant of the unit sphere. The red point corresponds to the node $n = 6$ and the green ones correspond to the nodes that share one of the $J_6 = 6$ edges of the region formed by the sixth node.

where $\delta\Omega_n$ is the boundary of the region Ω_n and $\mathbf{n}_\ell$ is the normal vector at region boundary on $\mathbb{S}^2$.

Assuming that the region Ω_n is a polygon with J_n sides, then the integral can be rewritten as the sum of the J_n integrals over the edges of the n'th region,

$$Q_{g,n}^{\mathrm{AFP}} = \frac{T_g}{\omega_n}\sum_{j=1}^{J_n}\int_{\delta\Omega_{n,j}} d\ell \nabla_t \Psi_g(\Omega)\cdot \boldsymbol{n}_\ell \ . \tag{30}$$

The central finite-difference is used to approximate the derivative on each edge of the polygon, and this derivate is assumed to be constant over the entire edge. The previous expression can be approximated by

$$Q_{g,n}^{\mathrm{AFP}} = \frac{T_g}{\omega_n}\sum_{j=1}^{J_n}\ell_{n,j}\left[\frac{\Psi_{g,m_{n,j}}-\Psi_{g,n}}{\Delta x_{n,j}}\right] , \tag{31}$$

where

$\ell_{n,j}$ = length of the j'th edge, which is an arc on the unit sphere

$\Psi_{g,n} = \Psi_g(\Omega_n)$ = angular flux along node n

$\Psi_{g,m_{n,j}}$ = angular flux of the node $m_{n,j}$ that shares the edge j with the node n

$\Delta x_{n,j}$ = length of the arc between the two nodes n and m.

Let us introduce a general parameter $\gamma_{n,m_{n,j}}$ that includes both $\ell_{n,j}$ and $\Delta x_{n,j}$ and is associated with the shared edge between the nodes n. This parameter will be used as an adjustment parameter to enforce moment preservation and will differ from the ratio of $\ell_{n,j}$ and $\Delta x_{n,j}$ that it substitutes. The property $\gamma_{n,m} = \gamma_{m,n}$ is enforced, such as each edge is associated with a unique coefficient $\gamma_{n,m}$ with $n < m$. The discretized AFP operator takes the form

$$Q_{g,n}^{\mathrm{AFP}} = \frac{T_g}{\omega_n}\sum_{j=1}^{J_n}\gamma_{n,m_{n,j}}\left[\Psi_{g,m_{n,j}}-\Psi_{g,n}\right] . \tag{32}$$

Figure 3 shows an example of how these relations are defined between adjacent regions on the unit sphere. A Voronoi tessellation, based on the set of quadrature nodes, was constructed over the unit sphere, such as an arbitrary point on $\mathbb{S}^2$ belongs to the closest node Ω_n. The resulting grid was used to establish which regions share which edge. Voronoi grids for product, level-quadrature, and Lebedev quadrature are shown in Fig. 2.

The values of the $\gamma_{n,m}$ coefficients are fixed to enforce the preservation of the zeroth and first moments of the flux. Note that, regardless of the value of the $\gamma_{n,m}$ values, the discretized AFP operator preserves the null space, which means that any isotropic angular flux leads to zero. Following that the spherical harmonics are eigenfunctions of the Laplace operator[10], i.e.,

$$\nabla_\Omega^2 R_{\ell_p}^{m_p}(\Omega) = -\ell_p\left(\ell_p+1\right)R_{\ell_p}^{m_p}(\Omega) , \tag{33}$$

the preservation of the spherical harmonics moments of the AFP operator requires the enforcement of

$$\begin{aligned}&\int_{\mathbb{S}^2} d^2\Omega R_{\ell_p}^{m_p}(\Omega) Q_g^{\mathrm{AFP}}(\Omega)\\ &= -T_g\ell_p\left(\ell_p+1\right)\int_{\mathbb{S}^2} d^2\Omega R_{\ell_p}^{m_p}(\Omega)\Psi_g(\Omega) \ .\end{aligned} \tag{34}$$

The zeroth and the three first moments of the AFP operator are therefore given by

$$\int_{\mathbb{S}^2} d^2\Omega Q_g^{\mathrm{AFP}}(\Omega) = 0$$

and

$$\int_{\mathbb{S}^2} d^2\Omega\Omega Q_g^{\mathrm{AFP}}(\Omega) = -2T_g\int_{\mathbb{S}^2} d^2\Omega\Omega\Psi_g(\Omega), \tag{35}$$

and should be preserved by the discretized AFP operator, such as

$$\sum_{n=1}^{N_d}\omega_n Q_{g,n}^{\mathrm{AFP}} = 0$$

and

$$\sum_{n=1}^{N_d}\omega_n\Omega_n Q_{g,n}^{\mathrm{AFP}} = -2T_g\sum_{n=1}^{N_d}\omega_n\Omega_n\Psi_{g,n} \ , \tag{36}$$

with $\boldsymbol{\Omega}_n = (\mu_n, \eta_n, \xi_n)$.

The finite-difference scheme given by Eq. (32) preserves the zeroth moment of the AFP operator for any value of $\gamma_{n,m}$. To find the parameters $\gamma_{n,m}$ that preserve the three discretized first moments of the flux, the methodology proposed by Morel et al.[10] was used. Explicit equations for $\gamma_{n,m}$ were obtained by defining the following complete basis:

$$\boldsymbol{\psi}_{g,k} = \left(\delta_{1,k}, \delta_{2,k}, ..., \delta_{N_d,k}\right) \ , \tag{37}$$

where $\delta_{n,k}$ is the Kronecker delta. Substituting it and Eq. (32) in the rightmost expression in Eq. (36) for each $k = 1, N_d$, one obtains N_d equations of the form

$$\sum_{j=1}^{J_k} \gamma_{k,m_{k,j}} \left[\Omega_{m_{k,j}} - \Omega_k\right] = -4\omega_k \Omega_k \ , \tag{38}$$

where $\Omega_{m_{k,j}}$ is the coordinates of the node that share the edge j with node k for a total of $3N_d$ equations.

Regardless of the choice of quadrature, it leads to an overdetermined linear system of equations since the number of unknown parameters $\gamma_{n,m}$ with $n < m$, which is equal to the total number of edges between nodes N_{edges}, is smaller than the total number of equations $3N_d$. This can be deduced from Euler's polyhedron formula, which states that the sum of vertices $N_{vertices}$, edges N_{edges}, and faces N_d in a convex polyhedron, as the one formed by the quadrature nodes, is given by Euler characteristic $\chi = 2$, and from the fact that there are at least three edges connecting at each vertex, such as $2N_{edges} \geq 3N_{vertices}$.[35] It follows that

$$N_{edges} = N_d + N_{vertices} - 2 \leq 3N_d - 6 \leq 3N_d \ . \tag{39}$$

Fortunately, with any quadrature set we have tested, ranging from product, level symmetric, and Lebedev quadrature, the resulting system contains redundant equations, likely due to symmetry in these quadrature sets. Solving this system using the Moore-Penrose inverse,[36,37] also called pseudoinverse, gives an exact solution for $\gamma_{n,m}$ such that all the three N_d equations are simultaneously satisfied. Since the system's matrix has a full column rank, the solution is unique.

It has been observed that all values of $\gamma_{n,m}$ are positive and respect the quadrature set symmetries. These observations will require further investigations to assert the properties of quadrature (e.g., required symmetries) compatible with our approach, i.e., leading to an exact solution rather than an inexact least-squares solution, which is usually expected with the pseudoinverse.

Using the calculated zeroth and first moment–preserving coefficients $\gamma_{n,m}$, the resulting mapping matrix is given by

$$\mathcal{M}_{n,m} = \begin{cases} -\dfrac{1}{\omega_n} \sum_{j=1}^{J_n} \gamma_{n,m_{n,j}} & \text{if } n = m \\ \dfrac{\gamma_{n,m}}{\omega_n} & \text{if } m \in \{m_{n,j} : j = 1, J_n\} \\ 0 & \text{otherwise} \end{cases} \ . \tag{40}$$

The produced matrix is negative, semidefinite, and monotone. The presented methodology, applied to product quadrature with Chebychev azimuthal quadrature, reproduces the mapping matrix of the scheme from Morel et al.[10] given in the Appendix.

V. RESULTS

The benchmarks were based on pure electron transport in a water slab exposed by an infinitely wide, normally incident 10-MeV electron beam, unless noted otherwise. The energy domain was divided logarithmically into 40 energy groups, where the midpoint of the highest energy group was 10 MeV and the cutoff energy was 1 keV. Linear discontinuous schemes were used to deal with both the space and energy derivatives. A convergence criterion of 10^{-5} was used. Void boundary conditions were applied to the geometry boundaries.

Cross sections and stopping powers for elastic, impact ionization, and bremsstrahlung interactions were given by models described in Bienvenue et al.[16] The elastic cross sections were given by screened Mott cross sections based on the mixed uses of the unscreened Mott tabulation of Boschini[38] and the Rutherford formula with Molière screening,[15] with additional low-energy and low-Z corrections from Seltzer[39] and Kawrakow.[40] This elastic model becomes highly forward-peaked as the particle energy increases, providing an interesting study case for the presented angular discretization models. The impact ionization catastrophic cross sections were given by modified Møller cross sections taking into account binding energies[41,42] over the catastrophic domain. The soft collisional stopping powers were given by subtracting the stopping powers associated with the catastrophic collisional cross sections to the Bethe formula with density and shell corrections.[43] Finally, the bremsstrahlung catastrophic cross sections and soft stopping powers were obtained similarly using the tabulation of Seltzer and Berger.[44]

The calculation of the energy deposition cross section in each energy group included the addition of energy lost by the incoming electron (impact ionization and bremsstrahlung), by soft and catastrophic events, and by the subtraction of the energy gain by secondary particles (the knock-on electron and the bremsstrahlung photon). The methodology to compute the total energy deposition, which consisted of the energy deposited in each group and at the cutoff energy, can be found in Morel et al.[45] or Bienvenue et al.[16]

V.A. Comparison of Galerkin Quadrature Methods

In a conference paper,[24] Morel et al. compared two Galerkin quadratures methods for a product quadrature defined over the unit sphere that consisted of inverting either the discrete-to-moment **D** or the moment-to-discrete **M**, as presented in Sec. III. Their results showed that these methods give similar flux solutions for a benchmark in which an isotropic boundary source is defined. Recently, Shands et al. proposed additional comparisons of these two methods with a novel Galerkin quadrature method over similar benchmarks, giving similar conclusions.[3] However, it was observed that one method was superior in some cases with quadrature defined over the unit sphere.

The 1D Cartesian geometry was used with the Lebedev quadrature. Unlike most 1D slab geometry calculations in literature, the angular domain was not simplified from the unit sphere to the main direction cosine domain between −1 and 1. The spherical harmonics must be kept as the interpolation basis rather than the Legendre polynomials, and quadrature on the unit sphere is required, as is done in 3D Cartesian geometry. This method aims to test angular discretization on the unit sphere without relying on costly multidimensional calculations or incurring errors introduced by such calculations, such as ray effects.

The geometry domain, an infinitely wide 5-cm slab, was divided into 40 voxels. The Galerkin scheme was used for the AFP operator. The first comparison consisted of a benchmark with a 10-MeV isotropic source defined between 2 cm and 3 cm, while the second one used a normally incident 10-MeV beam. As shown in Fig. 4, for isotropic sources, both methods gave similar results for any quadrature order. This was coherent with the result in Morel et al.[24] However, for the normally incident boundary source, the $\mathbf{D} = \mathbf{M}^{-1}$ energy deposition results were less accurate than the $\mathbf{M} = \mathbf{D}^{-1}$ ones at any quadrature order. Notably, the S_9 solution presented a huge overestimation of the deposited energy between a 0-cm and 1-cm depth. Even at high quadrature order (S_{23}), while seemingly converging toward the $\mathbf{M} = \mathbf{D}^{-1}$ solution, the $\mathbf{D} = \mathbf{M}^{-1}$ solution still exhibited significant spurious oscillations. The $\mathbf{M} = \mathbf{D}^{-1}$ Galerkin quadrature method was therefore used for the following results.

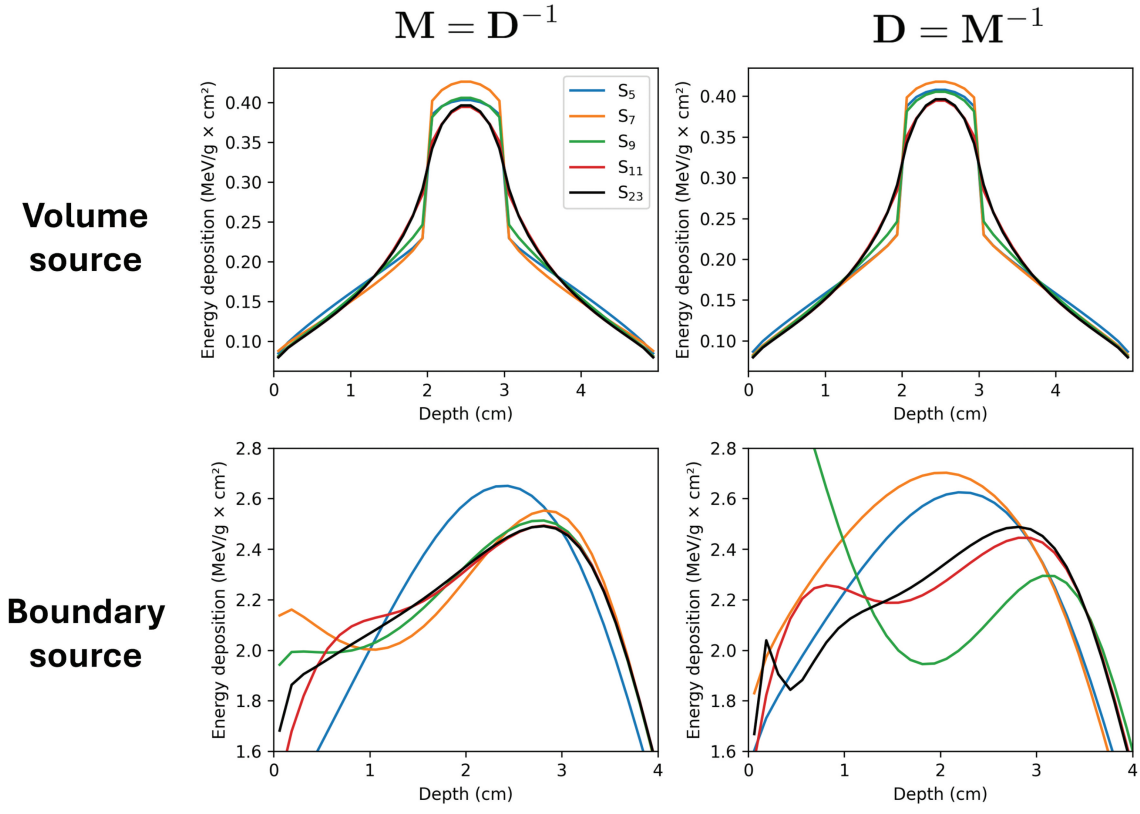

Fig. 4. Comparison of two Galerkin quadrature methods for different quadrature orders for benchmark with (top) isotropic source or (bottom) normally incident source.

V.B. AFP Finite-Difference Schemes

The first benchmark compared the Galerkin and Morel 1D finite-difference discretization of the AFP term[8] in 1D Cartesian geometry using the Gauss–Lobatto quadrature. The geometry domain, an infinitely wide 5-cm slab, was divided into 40 voxels. The Galerkin and finite-difference mapping matrix of the S_6 case, provided to highlight their properties, are respectively given by

$$\mathcal{M}_6^G = \begin{bmatrix} 0.0 & 20.2828 & -8.07237 & 4.48937 & -2.69983 & 1.0 \\ 3.57273 & 5.0 & 8.22289 & -2.67431 & 1.35425 & -0.475562 \\ -0.969902 & 5.60893 & 5.0 & 6.64575 & -1.82418 & 0.539401 \\ 0.539401 & -1.82418 & 6.64575 & 5.0 & 5.60893 & -0.969902 \\ -0.475562 & 1.35425 & -2.67431 & 8.22289 & 5.0 & 3.57273 \\ 1.0 & -2.69983 & 4.48937 & -8.07237 & 20.2828 & 0.0 \end{bmatrix} \tag{41}$$

and

$$\mathcal{M}_6^{FD} = \begin{bmatrix} -8.51264 & 8.51264 & 0.0 & 0.0 & 0.0 & 0.0 \\ 1.49946 & -5.42257 & 3.92311 & 0.0 & 0.0 & 0.0 \\ 0.0 & 2.676 & -5.92681 & 3.25081 & 0.0 & 0.0 \\ 0.0 & 0.0 & 3.25081 & -5.92681 & 2.676 & 0.0 \\ 0.0 & 0.0 & 0.0 & 3.92311 & -5.42257 & 1.49946 \\ 0.0 & 0.0 & 0.0 & 0.0 & 8.51264 & -8.51264 \end{bmatrix}. \tag{42}$$

The finite-difference matrix is clearly monotone since the row's off-diagonal components are positive and the diagonal components are negative, and it is diagonally dominant since the sum of the row's off-diagonal components is equal to the absolute value of the diagonal components. These properties were not shared by the Galerkin matrix. Along each line n of the Galerkin matrix, corresponding to the incoming angular flux direction, the main scattering events were $n \rightarrow n-1$ (for $n \neq 1$) and $n \rightarrow n+1$ (for $n \neq N_d$), as in the finite-difference case, but farther away from the diagonal, the values sign oscillated. The negative sign for a nondiagonal element $m \neq n$ is not desirable since it implies that the flux Ψ_n along the direction μ_n scatter, such as there is a reduction along the direction μ_m, does not make any physical sense. On the contrary, the finite-difference matrix was more physically robust since the flux Ψ_n along the direction μ_n scatter, such as the flux lost at $m = n$, was redistributed along the directions $m \neq n$.

The energy deposition solutions for a quadrature order varying from 4 to 12 are shown in Fig. 5. The reference

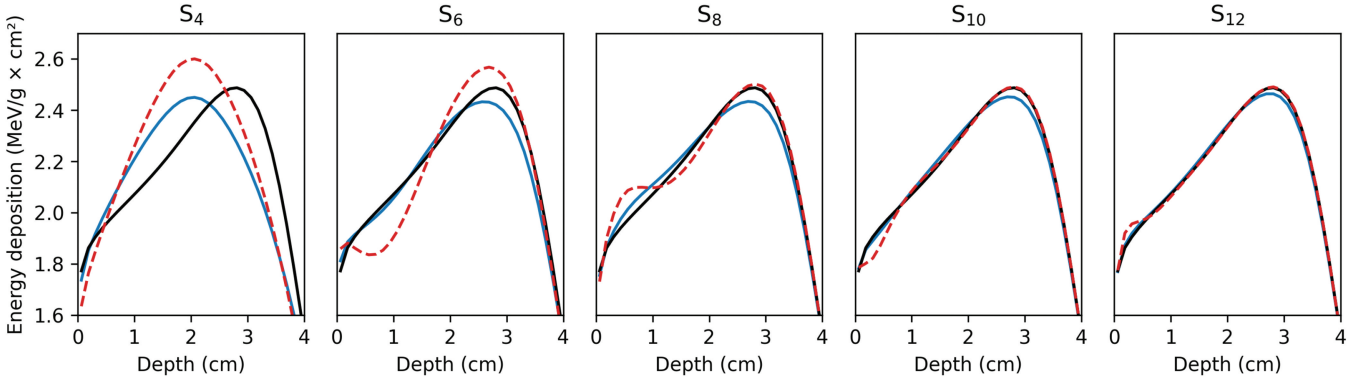

Fig. 5. Comparison of energy deposition profiles using (red) Galerkin and (blue) finite-difference schemes for the FP operator based on the Gauss–Lobatto quadrature in 1D Cartesian geometry. The (black) reference solution was obtained using the S_{26} finite-difference scheme.

solution was obtained with the S_{26} finite-difference scheme. The solution using the Galerkin scheme presented significant nonphysical oscillations due to the discussed lack of monotonicity of the mapping matrix $\mathcal{M}$. These oscillations can be damped by increasing the quadrature order, but some artifacts can be persistent, as shown by the S_{12} case near $x = 0$ cm. This scheme, used jointly with the Galerkin quadrature method, preserved N_d moments of the AFP operator.[4] It made the Galerkin scheme a more accurate moment representation of the AFP operator than the finite-difference scheme, which preserved only the zeroth and first moments.

This explains the better agreement of the low-order Galerkin scheme near $x = 3$ cm with the reference solution. The finite-difference scheme was more robust for any quadrature order since it eliminated the spurious oscillations in the solution. As the quadrature order increased, both the Galerkin and finite-difference schemes tended toward the same solution.

The second benchmark compared the Galerkin and the multidimensional finite-difference discretization of the AFP term in 1D Cartesian geometry using the Lebedev quadrature. The geometry domain, an infinitely wide 5-cm slab, was divided into 40 voxels. The energy deposition solutions for quadrature order varying from 5 to 13 are shown in Fig. 6. The solution using the Galerkin scheme exhibited oscillations similar to the one with the Gauss–Lobatto, but at different locations. This shows that such behavior is difficult to predict for a given quadrature choice. As with the 1D AFP finite-difference scheme, the multidimensional AFP one provided a solution free of such oscillations at the cost of the enforcement of high-order spherical harmonics moments of the AFP operator.

The third benchmark compared the Galerkin and the multidimensional finite-difference discretization of the AFP term in 3D Cartesian geometry using the Lebedev quadrature. The Cartesian geometry domain, whose size was $5 \times 5 \times 1.5$ cm along each axis, was divided into 20, 20, and 6 voxels. The source of electrons was defined over all the surface y–z at $x = 0$ and produced particles in direction $\mu = 1$. The Galerkin and finite-difference mapping matrix had, respectively, the same properties as in the 1D case.

The energy deposition solution for quadrature order varying from 5 to 13 is shown in Fig. 7. The solution using the Galerkin scheme presented, as expected, nonphysical oscillations along both the x- and y-spatial axis. As in the 1D case, increasing the quadrature order improved the overall monotonicity, but did not solve it. The finite-difference method, which preserved the zeroth and the three first moments of the AFP operator, eliminated any spurious oscillations of the Galerkin scheme.

The newly developed method permits monotonicity-enforcing AFP operator treatment with an optimal quadrature. This is very useful for particle transport since it diminishes greatly the number of directions required to achieve a specific angular accuracy and then improves running times. For example, the speedup of the Lebedev quadrature for S_5, S_9, and S_{17} compared to the product quadrature for S_4, S_8, and S_{16} are, respectively, $\times 2.3$, 3.5, and $\times 4.7$. The Lebedev quadrature also offered a better distribution of nodes and desirable symmetries. The finite-difference schemes produced more predictable solutions than the Galerkin scheme since the oscillation intensity was difficult to evaluate before calculations.

It should be noted that this method does not address the issues related to the ray effect, which is caused by the forced fulfillment of the transport equation along the

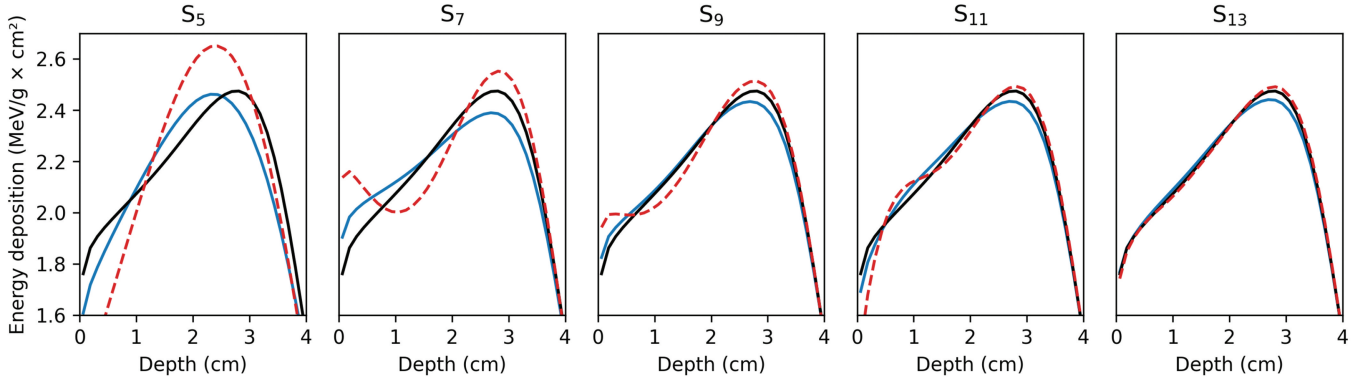

Fig. 6. Comparison of energy deposition profiles using (red) Galerkin and (blue) finite-difference schemes for the FP operator based on the Lebedev quadrature in 1D Cartesian geometry. The (black) reference solution was obtained using the S_{23} finite-difference scheme.

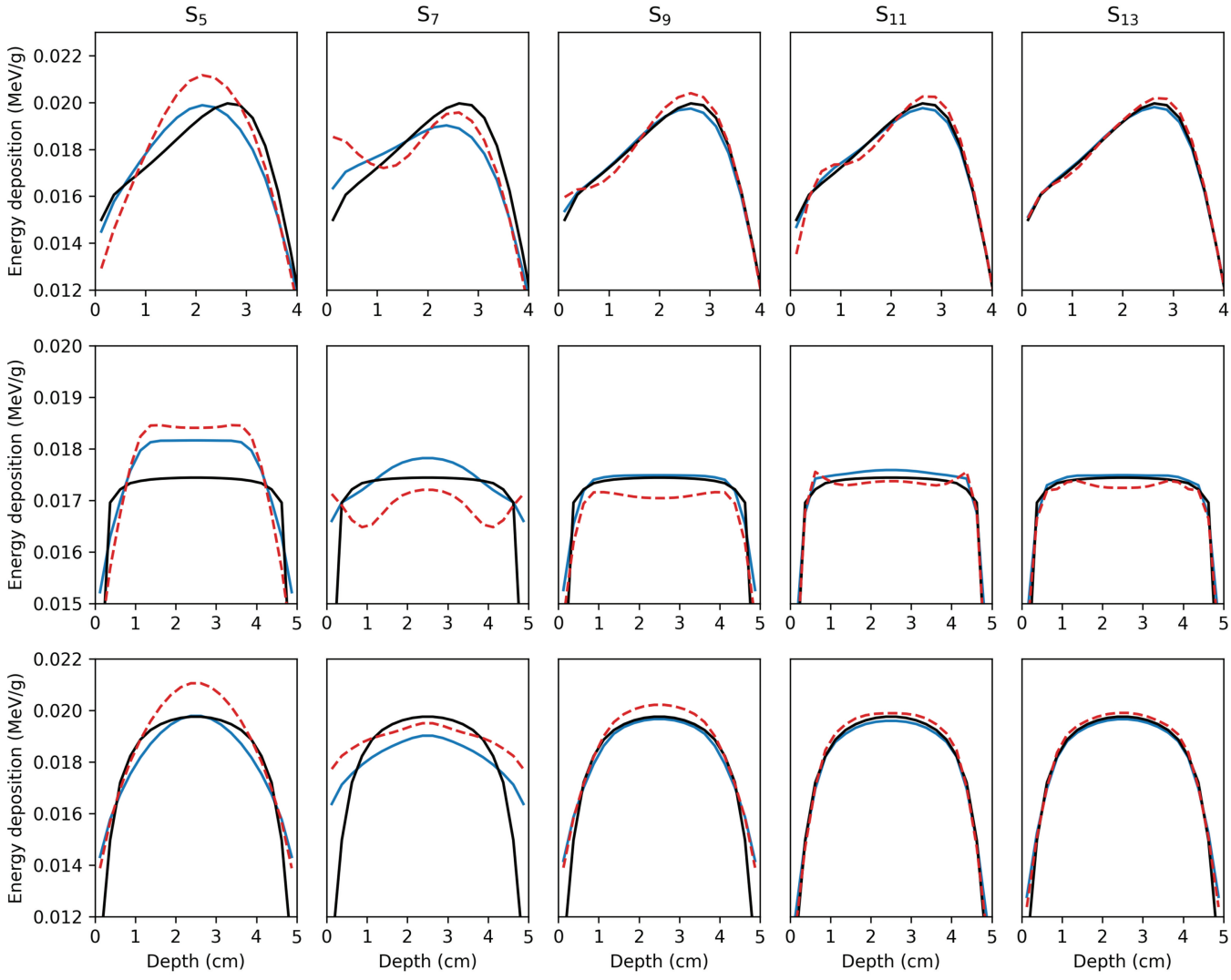

Fig. 7. Comparison of energy deposition profiles along (a) $y = 2.5$ cm, (b) $x = 1.25$ cm, and (c) $x = 2.5$ cm using (red) Galerkin and (blue) finite-difference schemes for the FP operator based on the Lebedev quadrature in 3D Cartesian geometry. The (black) reference solution was obtained using the S_{19} finite-difference scheme.

discrete set of directions only and the lack of rotational invariance of the streaming operator.[46]

VI. CONCLUSION

In this work, a methodology to produce monotone schemes for the multidimensional AFP operator, compatible with nonorthogonal quadrature sets and preserving the null space, the zeroth, and the first moments of the analytical AFP operator, was introduced. These schemes were used to treat the forward-peaked component of the elastic scattering with the Boltzmann transport equation. Results for 1D and 3D geometry calculations showed that these schemes eliminated spurious oscillations related to such scattering. Further investigations will be required to assess the properties of the quadrature set, such as rotational symmetries compatible with the proposed approach.

APPENDIX

FINITE-DIFFERENCE SCHEME FOR THE MULTIDIMENSIONAL AFP OPERATOR

The 2D finite-difference scheme using product quadrature with Chebychev azimuthal quadrature from Morel et al. is given by[10]

$$\mathcal{M}_{x,y} = \begin{cases} -C_n - D_{n,i} & \text{if } n = m \text{ and } i = j \\ C_n^- & \text{if } n = m+1 \text{ and } i = j \\ C_n^+ & \text{if } n = m-1 \text{ and } i = j \\ D_{n,i}^- & \text{if } n = m \text{ and } i = j+1 \\ D_{n,i}^+ & \text{if } n = m \text{ and } i = j-1 \\ 0 & \text{otherwise} \end{cases} , \tag{A.1}$$

with $x = i + N(n-1)$ and $y = j + N(m-1)$, where the C-terms are defined by Eq. (24) and the D-terms are defined by

$$D_{n,i}^- = \frac{\gamma_n}{w(\omega_i - \omega_{i-1})\left(1-\mu_n^2\right)} , \tag{A.2}$$

$$D_{n,i}^+ = \frac{\gamma_n}{w(\omega_{i+1} - \omega_i)\left(1-\mu_n^2\right)} , \tag{A.3}$$

and

$$D_{n,i} = D_{n,i}^- + D_{n,i}^+ . \tag{A.4}$$

The weights of the Chebychev quadrature are given by

$$w = \frac{\pi}{N} \quad \text{and} \quad \omega_i = \frac{(2i-1)\pi}{2N} , \tag{A.5}$$

while the coefficients γ_n are given by

$$\gamma_n = \frac{\pi^2}{2N\left(1-\cos\left(\frac{\pi}{N}\right)\right)}\left[2(1-\mu_n^2) + \frac{\sqrt{1-\mu_n^2}}{\omega_n}\left(C_{n+1/2}d_{n+1/2} - C_{n-1/2}d_{n-1/2}\right)\right] , \tag{A.6}$$

with

$$d_{n+1/2} = \frac{\sqrt{1-\mu_{n+1}^2} - \sqrt{1-\mu_n^2}}{\mu_{n+1} - \mu_n} . \tag{A.7}$$

The 3D finite-difference scheme is given by

$$\mathbb{M}_{x,y} = \begin{cases} -C_n - E_{n,i} & \text{if } n = m \text{ and } i = j \\ C_n^- & \text{if } n = m+1 \text{ and } i = j \\ C_n^+ & \text{if } n = m-1 \text{ and } i = j \\ E_{n,i}^- & \text{if } n = m \text{ and } \{i = j+1 \text{ or } (i = 1 \text{ and } j = 2N)\} \\ E_{n,i}^+ & \text{if } n = m \text{ and } \{i = j-1 \text{ or } (i = 2N \text{ and } j = 1)\} \\ 0 & \text{otherwise} \end{cases} , \tag{A.8}$$

with $x = i + 2N(n-1)$ and $y = j + 2N(m-1)$, where the C-terms are defined by Eq. (24) and the E-terms are defined by

$$E_{n,i}^{-} = \begin{cases} \dfrac{\gamma_n}{w(\omega_i - \omega_{i-1})(1-\mu_n^2)} & \text{if } i \neq 1 \\ \dfrac{\gamma_n}{w(2\pi + \omega_1 - \omega_{2N})(1-\mu_n^2)} & \text{otherwise} \end{cases}, \tag{A.9}$$

$$E_{n,i}^{+} = \begin{cases} \dfrac{\gamma_n}{w(\omega_{i+1} - \omega_i)(1-\mu_n^2)} & \text{if } i \neq 2N \\ \dfrac{\gamma_n}{w(2\pi + \omega_1 - \omega_{2N})(1-\mu_n^2)} & \text{otherwise} \end{cases}, \tag{A.10}$$

and

$$E_{n,i} = E_{n,i}^{-} + E_{n,i}^{+} \quad . \tag{A.11}$$

Disclosure Statement

No potential conflict of interest was reported by the authors.

Funding

This work was supported by the Natural Sciences and Engineering Research Council of Canada [RGPIN-2022-03810] and the Natural Sciences and Engineering Research Council of Canada [RGPIN-2021-03899].

ORCID

Charles Bienvenue http://orcid.org/0000-0001-9219-2131

References

1. J. E. MOREL, "A Hybrid Collocation-Galerkin-S_n Method for Solving the Boltzmann Transport Equation," *Nucl. Sci. Eng.*, **101**, *1*, 72 (1989); http://dx.doi.org/10.13182/NSE89-4.
2. S. D. PAUTZ and M. L. ADAMS, "An Asymptotic Study of Discretized Transport Equations in the Fokker-Planck Limit," *Nucl. Sci. Eng.*, **140**, *1*, 51 (2002); http://dx.doi.org/10.13182/NSE02-A2244.
3. E. W. SHANDS et al., "A New Galerkin Quadrature Method Not Requiring a Matrix Inverse," *Nucl. Sci. Eng.* (2024) (accepted for publication); http://dx.doi.org/10.1080/00295639.2024.2385220.
4. Y. AZMY et al., "Advances in Discrete-Ordinates Methodology," *Nuclear Computational Science*, E. W. LARSEN and J. E. MOREL, Eds. pp. 1–84, Springer Nature (2009).
5. J. S. WARSA and A. K. PRINJA, "Moment-Preserving S_N Discretizations for the One-Dimensional Fokker-Planck Equation," Los Alamos National Laboratory (2012).
6. K. D. LATHROP, "Ray Effects in Discrete Ordinates Equations," *Nucl. Sci. Eng.*, **32**, *3*, 357 (1968); http://dx.doi.org/10.13182/NSE68-4.
7. M. LANDESMAN and J. MOREL, "Angular Fokker-Planck Decomposition and Representation Techniques," *Nucl. Sci. Eng.*, **103**, *1*, 1 (1989); http://dx.doi.org/10.13182/NSE89-A23655.
8. J. E. MOREL, "An Improved Fokker-Planck Angular Differencing Scheme," *Nucl. Sci. Eng.*, **89**, *2*, 131 (1985); http://dx.doi.org/10.13182/NSE85-A18187.
9. L. A. POVEDA and P. PEIXOTO, "On Pointwise Error Estimates for Voronoï-Based Finite Volume Methods for the Poisson Equation on the Sphere," *Adv. Comput. Math.*, **49**, *3*, 36 (2023); http://dx.doi.org/10.1007/s10444-023-10041-3.
10. J. E. MOREL et al., "A Discretization Scheme for the Three-Dimensional Angular Fokker-Planck Operator," *Nucl. Sci. Eng.*, **156**, *2*, 154 (2007); http://dx.doi.org/10.13182/NSE07-A2693.
11. K. PRZYBYLSKI and J. LIGOU, "Numerical Analysis of the Boltzmann Equation Including Fokker-Planck Terms," *Nucl. Sci. Eng.*, **81**, *1*, 92 (1982); http://dx.doi.org/10.13182/NSE82-A19597.
12. G. POMRANING, "The Fokker-Planck Operator as an Asymptotic Limit," *Math. Models Methods Appl. Sci.*, **2**, *1*, 21 (1992); http://dx.doi.org/10.1142/S021820259200003X.
13. J. MOREL, "Fokker–Planck Calculations Using Standard Discrete Ordinates Transport Codes," *Nucl. Sci. Eng.*, **79**, *4*, 340 (1981); http://dx.doi.org/10.13182/NSE79-340.
14. A. HÉBERT, *Applied Reactor Physics*, Presses Inter Polytechnique (2009).
15. L. LORENCE JR, J. MOREL, and G. VALDEZ, "Physics Guide to CEPXS: A Multigroup Coupled Electron-Photon Cross-Section Generating Code," Sandia National Laboratories (1989).
16. C. BIENVENUE et al., "Toward Highly Accurate Multigroup Coupled Photon-Electron-Positron Cross-Sections for the Boltzmann Fokker-Planck Equation," *J. Comput. Phys.*, **524**, 113740 (2025); http://dx.doi.org/10.1016/j.jcp.2025.113740.

17. M. S. LAZO and J. MOREL, "A Linear Discontinuous Galerkin Approximation for the Continuous Slowing Down Operator," *Nucl. Sci. Eng.*, **92**, *1*, 98 (1986); http://dx.doi.org/10.13182/NSE86-A17870.
18. C. BIENVENUE and A. HÉBERT, "High-Order Diamond Differencing Schemes for the Boltzmann Fokker-Planck Equation in 1D and 2D Cartesian Geometries," *Ann. Nucl. Energy*, **171**, 109032 (2022); http://dx.doi.org/10.1016/j.anucene.2022.109032.
19. C. BIENVENUE et al., "Adaptive Gradient-Driven Coupled Linear Schemes and Their Usefulness for Charged Particle Transport," presented at the Int. Conf. on Mathematics and Computational Methods Applied to Nuclear Science and Engineering (M&C 2023) (2023).
20. M. CARO and J. LIGOU, "Treatment of Scattering Anisotropy of Neutrons Through the Boltzmann-Fokker–Planck Equation," *Nucl. Sci. Eng.*, **83**, *2*, 242 (1983); http://dx.doi.org/10.13182/NSE83-A18217.
21. J. MOREL, "On the Validity of the Extended Transport Cross-Section Correction for Low-Energy Electron Transport," *Nucl. Sci. Eng.*, **71**, *1*, 64 (1979); http://dx.doi.org/10.13182/NSE79-A20332.
22. C. R. DRUMM et al., "An Analysis of the Extended-Transport Correction with Application to Electron Beam Transport," *Nucl. Sci. Eng.*, **155**, *3*, 355 (2007); http://dx.doi.org/10.13182/NSE07-A2668.
23. W. H. REED, "Spherical Harmonic Solutions of the Neutron Transport Equation from Discrete Ordinate Codes," *Nucl. Sci. Eng.*, **49**, *1*, 10 (1972); http://dx.doi.org/10.13182/NSE72-A22523.
24. J. E. MOREL et al., "Comparison of Two Galerkin Quadrature Methods," *Nucl. Sci. Eng.*, **185**, *2*, 325 (2017); http://dx.doi.org/10.1080/00295639.2016.1272383.
25. R. SANCHEZ and J. RAGUSA, "On the Construction of Galerkin Angular Quadratures," *Nucl. Sci. Eng.*, **169**, *2*, 133 (2011); http://dx.doi.org/10.13182/NSE10-31.
26. C. DRUMM et al., "Least-Squares Finite-Element Algorithms in the SCEPTRE Radiation Transport Code," presented at the Int. Conf. on Mathematics and Computational Methods Applied to Nuclear Science and Engineering (M&C 2011) (2011).
27. C. R. DRUMM, W. C. FAN, and S. D. PAUTZ, "Specializations in the SCEPTRE Code for Charged-Particle Transport," Sandia National Laboratories (2018).
28. A. MCLAREN, "Optimal Numerical Integration on a Sphere," *Math. Comput.*, **17**, *84*, 361 (1963); http://dx.doi.org/10.1090/S0025-5718-1963-0159418-2.
29. B. G. CARLSON, "A Method of Characteristics and Other Improvements in Solution Methods for the Transport Equation," *Nucl. Sci. Eng.*, **61**, *3*, 408 (1976); http://dx.doi.org/10.13182/NSE76-A26927.
30. V. I. LEBEDEV, "Values of the Nodes and Weights of Ninth to Seventeenth Order Gauss-Markov Quadrature Formulae Invariant Under the Octahedron Group with Inversion," *USSR Comput. Math. Math. Phys.*, **15**, *1*, 44 (1975); http://dx.doi.org/10.1016/0041-5553(75)90133-0.
31. V. I. LEBEDEV, "Quadratures on a Sphere," *USSR Comput. Math. Math. Phys.*, **16**, *2*, 10 (1976); http://dx.doi.org/10.1016/0041-5553(76)90100-2.
32. V. I. LEBEDEV and D. N. LAIKOV, "A Quadrature Formula for the Sphere of the 131st Algebraic Order of Accuracy," *Doklady Mathe.*, **59**, *3*, 477 (1999).
33. A. HENNINK and D. LATHOUWERS, "A Discontinuous Galerkin Method for the Mono-Energetic Fokker-Planck Equation Based on a Spherical Interior Penalty Formulation," *J. Comput. Appl. Math.*, **330**, 253 (2018); http://dx.doi.org/10.1016/j.cam.2017.08.019.
34. G. DZIUK and C. M. ELLIOTT, "Finite Element Methods for Surface PDEs," *Acta Numer.*, **22**, 289 (2013); http://dx.doi.org/10.1017/S0962492913000056.
35. D. ZWILLINGER, *CRC Standard Mathematical Tables and Formulas*, Chapman and Hall/CRC (2018).
36. R. PENROSE, "A Generalized Inverse for Matrices," *Mathematical Proceedings of the Cambridge Philosophical Society*, Vol. 51, pp. 406–413, Cambridge University Press (1955).
37. Å. BJÖRCK, *Numerical Methods for Least Squares Problems*, SIAM (2024).
38. M. BOSCHINI, "An Expression for the Mott Cross Section of Electrons and Positrons on Nuclei with Z up to 118," *Radiat. Phys. Chem.*, **90**, 39 (2013); http://dx.doi.org/10.1016/j.radphyschem.2013.04.020.
39. S. M. SELTZER, "An Overview of ETRAN Monte Carlo Methods," *Monte Carlo Transport of Electrons and Photons*, T. M. JENKINS, W. R. NELSON, and A. RUNDI, Eds. pp. 153–181, Springer Nature (1988).
40. I. KAWRAKOW, "Improved Modeling of Multiple Scattering in the Voxel Monte Carlo Model," *Med. Phys.*, **24**, *4*, 505 (1997); http://dx.doi.org/10.1118/1.597933.
41. S. M. SELTZER, "Cross Sections for Bremsstrahlung Production and Electron-Impact Ionization," *Monte Carlo Transport of Electrons and Photons*, T. M. JENKINS, W. R. NELSON, and A. RUNDI, Eds. pp. 81–114, Springer Nature (1988).
42. S. PERKINS and D. CULLEN, "The Livermore Electron Impact Ionization Data Base," Lawrence Livermore National Laboratory (1989).
43. F. SALVAT and P. ANDREO, "SBETHE: Stopping Powers of Materials for Swift Charged Particles from the Corrected

Bethe Formula," *Comput. Phys. Commun.*, **287**, 108697 (2023); http://dx.doi.org/10.1016/j.cpc.2023.108697.

44. S. M. SELTZER and M. J. BERGER, "Bremsstrahlung Energy Spectra from Electrons with Kinetic Energy 1 keV–10 GeV Incident on Screened Nuclei and Orbital Electrons of Neutral Atoms with Z = 1–100," *At. Data Nucl. Data Tables*, **35**, *3*, 345 (1986); http://dx.doi.org/10.1016/0092-640X(86)90014-8.

45. J. MOREL et al., "A Hybrid Multigroup/Continuous-Energy Monte Carlo Method for Solving the Boltzmann-Fokker–Planck Equation," *Nucl. Sci. Eng.*, **124**, *3*, 369 (1996); http://dx.doi.org/10.13182/NSE124-369.

46. J. E. MOREL et al., "Analysis of Ray-Effect Mitigation Techniques," *Nucl. Sci. Eng.*, **144**, *1*, 1 (2003); http://dx.doi.org/10.13182/NSE01-48.